Small-Signal Transfer Functions of the Classical Boost Converter Supplied by Ultracapacitor Banks

R.M.A.S. Rajakaruna
School of Electrical and Electronic Engineering
Nanyang Technological University
50 Nanyang Avenue, Singapore 679798

Abstract-**Ultracapacitor is an emerging device for energy storage that can replace batteries in some short-term applications. Due to the fact that the terminal voltage of an ultracapacitor varies with the level of energy stored, a power electronic converter with voltage boosting capability is usually needed at its terminals to interface with a load operating at a constant voltage. For the case of a classical boost dc-dc converter supplying a resistive load by drawing energy from a bank of ultracapacitors, the paper derives small-signal transfer functions by considering a time-varying steady-state. To reduce the complexity of resulting exact expressions of poles, highly accurate approximate expressions are also derived. Furthermore, it compares how the control characteristics change when a constant voltage source such as a battery replaces the ultracapacitor bank. A numerical example is presented to demonstrate the accuracy of the approximate values of poles and zeros and to describe how the poles and zeros vary with the duty ratio.**

I. Introduction

Ultracapacitor is an electrochemical type capacitor which offers large capacitances in the order of thousands of Farads but at a low rated voltage of about 2.5V [1-3]. The energy density of an ultracapacitor is about 100 times larger than a conventional electrolytic capacitor and its power density is about 10 times larger than a lead-acid battery. After its introduction to the market with large capacitances in the 1990's, it has become attractive for many industrial applications such as hybrid electric vehicles, power quality applications etc. because they are ideally suited to deliver high powers for a short duration of time [4-7]. Ultra-capacitors also have a number of other attractive properties, such as fast charge-discharge capability, longer life, no-maintenance and environmental friendliness due to no harmful emissions.

Despite the above attractive features, they also possess some undesirable features such as the low voltage rating, variable terminal voltage compared to batteries, larger series resistance compared to conventional capacitors, larger leakage current and higher nonlinearity in the capacitance with voltage. [1-3]. Due to the low rated voltage, many cells are connected in series to form a bank of capacitors that has sufficiently high rated voltage. In such banks of capacitors, voltage balancing by either active or passive balancing is also necessary to prevent damages of cells due to overvoltage. Furthermore, due to the variation of terminal voltage with the energy stored, a power electronic converter is usually needed at the terminal of a bank of ultracapacitors to convert it to a constant voltage source or a sink that is comparable with a battery. In order to minimize the number of series connected cells in the bank, a voltage boosting converter such as a classical boost converter [4] and flyback converter [7] is usually used in industrial applications.

In the case of a classical boost converter supplied by a constant voltage source such as a battery, some specific control problems such as the effects of Right Hand Plane (RHP) zero are discussed and some alternative converters have been proposed [8,9]. However, in designing a feedback controller for a converter supplied by a bank of ultracapacitors, it is found that there is hardly any literature available to understand the behaviour of the open-loop system. Therefore, the aim of this paper is to derive a small-signal model using fundamental concepts so that it can be used to understand the behaviour of the open-loop system before designing a feedback controller to achieve constant load voltage.

In section II of the paper, a simple electrical model of the switching circuit is used to derive the average state equation and to identify the characteristics of the steady-state. The small-signal transfer functions, the exact and approximate values of poles and zeros are then derived in section III. In order to demonstrate the accuracy of approximate values and to confirm the expected variations of poles and zeros with duty ratio, a numerical example is presented in section IV. Finally, the conclusions are presented in section V.

II. Average State Space Model

For the purpose of describing the terminal voltage vs. current characteristic of an ultracapacitor, many models have been developed in the past [1,10,11]. Despite the varying degree of accuracy of the models, almost all of them are too complex to be used in a small-signal analysis due to increased number of order of resulting differential equations. On the other hand, the objective of the analysis made in this paper is to identify the differences in control characteristics due to the replacement of the constant voltage source by a capacitor. Therefore, the ultracapacitor bank is modeled by an ideal capacitor in this paper. The effect of the equivalent series resistance (ESR) of the capacitors can be analyzed after studying the basic behaviour of the system. Figure 1 illustrates the electrical circuit diagram of the classical boost converter supplied by the bank of ultracapacitors. The stray resistances

1-4244-0737-0/07/$20.00 ©2007 IEEE

of all the circuit components have been neglected here to focus on the fundamental behaviour of the system. The converter consists of an input inductor L, output filter capacitor C_f, the switching transistor Sc and the diode D_c. The transistor S_c switches at a high frequency with a constant period T and a variable duty ratio d adjusted by the control circuit, not shown in Fig. 1. At the converter output terminals is the load resistor, R.

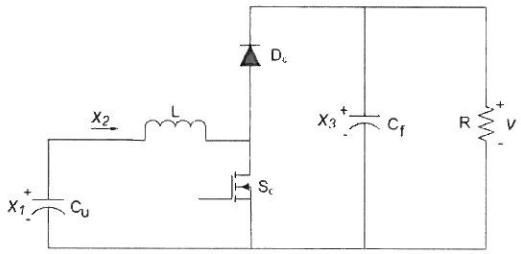

Fig. 1. Circuit diagram of the classical boost converter supplied by a bank of ultracapacitors.

A. Average System Model

In the circuit diagram given in Fig. 1, the three states x_1, x_2 and x_3 are selected as the voltage across the ultracapacitor bank, current through the input inductor and the voltage across the output filter capacitor respectively. The system differential equations for the period $d \cdot T$ during which the transistor is on can be written as,

$$\dot{x}_1 = (-1/C_u)x_2 \qquad \dot{x}_2 = (1/L)x_1 \qquad \dot{x}_3 = \left(-1/(RC_f)\right)x_3 \tag{1}$$

which can be expressed in matrix form as $\dot{x} = A_1 \cdot x$ where,

$$A_1 = \begin{pmatrix} 0 & -1/C_u & 0 \\ 1/L & 0 & 0 \\ 0 & 0 & -1/(RC_f) \end{pmatrix} \tag{2}$$

is the state matrix in the on-state of the transistor and

$$x = (x_1 \quad x_2 \quad x_3)^T \tag{3}$$

is the state vector. Similarly, for the off-state of the transistor with the duration $(1-d)T$, system differential equations are given by,

$$\dot{x}_1 = (-1/C_u)x_2 \qquad \dot{x}_2 = (1/L)(x_1 - x_3)$$
$$\dot{x}_3 = \left(1/C_f\right)(x_2 - x_3/R) \tag{4}$$

The corresponding state equation can therefore be written as $\dot{x} = A_2 \cdot x$ where,

$$A_2 = \begin{pmatrix} 0 & -1/C_u & 0 \\ 1/L & 0 & -1/L \\ 0 & 1/C_f & -1/(RC_f) \end{pmatrix} \tag{5}$$

is the state matrix in the transistor off-state. According to Middlebrook's state space averaging theory [12], the average values of state variables are given by

$$\dot{x} = \left[A_1 \cdot d + A_2 \cdot (1-d)\right] \cdot x \tag{6}$$

where the average state matrix $A = A_1 \cdot d + A_2 \cdot (1-d)$ can be expressed in terms of circuit parameters as,

$$A = \begin{pmatrix} 0 & -1/C_u & 0 \\ 1/L & 0 & -(1-d)/L \\ 0 & (1-d)/C_f & -1/(RC_f) \end{pmatrix} \tag{7}$$

Since the load voltage $V = x_3$ is the output variable, the output equation is given by $V = C \cdot x$ where $C = (0 \quad 0 \quad 1)$.

B. Steady-State Operating Points

1) DC Steady-State:

Since the derivatives of all the variables are zero at dc steady-state, dc steady-state relationships can be obtained by $\dot{X} = A \cdot X = 0$ where $X = (X_1 \quad X_2 \quad X_3)^T$ is the state vector at steady-state. By taking D as the duty-ratio at the steady-state, following dc steady-state equations can be derived.

$$X_2 = 0 \tag{8}$$

$$X_1 = (1-D)X_3 \tag{9}$$

$$X_3 = (1-D)R \cdot X_2 \tag{10}$$

According to (8)-(10), the only possible steady-state is when all state variables are zero. Since there is no source in the system, initial energy stored in the ultracapacitor bank, filter capacitor and inductor are used to supply the load. Hence, all the variables decay to zero with increasing time. Consequently, the system has no non-zero dc steady-state when the converter is in operation, i.e. for any value of D. Therefore, for the purpose of designing a controller using conventional methods, a small-signal analysis of the system can only be performed by considering a time-varying steady-state.

2) Time-Varying Steady-State:

Since the transfer functions of interest are from duty-ratio to state variables, the steady-state should be defined as the state of the system when the duty-ratio is constant. With a constant duty-ratio, the variables will change exponentially as demonstrated by computer simulation results in Section IV. Therefore, the state vector in steady-state can be expressed as

$$X(t) = (X_1 \quad X_2 \quad X_3)^T \cdot e^{-\omega_0 t} \tag{11}$$

where X_1, X_2, X_3 are the initial values of state variables and ω_0 is the steady-state frequency in rad/s. Then, substituting (11) in (6), following steady-state relationships can be obtained.

$$\omega_0 = \frac{X_2}{C_u X_1} \tag{12}$$

$$-\omega_0 X_2 = \frac{1}{L}\left[X_1 - (1-D)X_3\right] \tag{13}$$

$$-\omega_0 X_3 = \frac{1}{C_f}\left[X_2(1-D) - \frac{X_3}{R}\right] \tag{14}$$

Thus, if two out of five parameters X_1, X_2, X_3, D and ω_0 are

given, the other two parameters can be found using (12)-(14). By taking Laplace transform of (11), the frequency shift due to time-varying steady-state can be identified.

$$X(s)=(X_1 \quad X_2 \quad X_3)^T \cdot \frac{1}{(s+\omega_0)} \tag{15}$$

From (15), it is clear that the effect of exponentially varying steady-state is only to introduce a frequency shift by ω_0 to the values given by dc steady-state. The derivation of transfer functions can be performed as for a dc steady-state. However, the frequency of zeros should be corrected by deducting ω_0 as they depend on the state vector at steady-state. Since system poles do not depend on the steady-state, no such correction is needed for poles. It should be mentioned here that as in all small-signal analyses, the accuracy of the model drops as the operating point moves away from the assumed steady-state operating point.

III. Transfer Functions of Open-Loop System

In order to derive the small-signal transfer functions around the time-varying steady-state defined by $X=(X_1 \quad X_2 \quad X_3)^T$ and duty ratio D at time $t=0$, a small perturbation $\tilde{d}$ of duty ratio is introduced at time $t=0$ that causes corresponding changes of state variables given by $\tilde{x}_i$ where i = 1, 2, or 3. By substituting the instantaneous values of states and the duty ratio as $x_i = X_i + \tilde{x}_i$ and $d = D + \tilde{d}$, the state equation (6) can be rewritten as,

$$\dot{X}+\dot{\tilde{x}}=\left[A_1\cdot\left(D+\tilde{d}\right)+A_2\cdot\left(1-D-\tilde{d}\right)\right]\cdot(X+\tilde{x}) \tag{16}$$

By neglecting the product of small variations, the steady state values can be separated as,

$$\dot{X}=\left[A_1\cdot D+A_2\cdot(1-D)\right]\cdot X=A_0\cdot X$$

where $A_0=A_1\cdot D+A_2\cdot(1-D)$ is the initial state matrix at $t=0$ and it is given by (7) with all d terms replaced by D. As described in section II.B.2, in order to satisfy this equation, a time-varying steady-state has to be considered. The only difference it makes compared to a dc steady state is the frequency shift of ω_0 applied to zeros.

Similarly, the perturbed values of states are separated from (16) as,

$$\dot{\tilde{x}}=A_0\cdot\tilde{x}+\left[A_1-A_2\right]\cdot X\cdot\tilde{d} \tag{17}$$

By taking Laplace transform of (17), perturbed values of states are given by,

$$\tilde{x}=(sI-A_0)^{-1}\cdot\left[A_1-A_2\right]\cdot X\cdot\tilde{d} \tag{18}$$

where s is the complex frequency, I is a 3x3 unit matrix. The state transfer functions with respect to duty ratio can then be derived as,

$$\left[G_1(s)\ G_2(s)\ G_3(s)\right]^T=\left[\frac{\tilde{x}_1(s)}{\tilde{d}(s)}\ \frac{\tilde{x}_2(s)}{\tilde{d}(s)}\ \frac{x_3(s)}{d(s)}\right]^T \tag{19}$$
$$=\left[s\cdot I-A_0\right]^{-1}(A1-A2)X$$

If the state transfer functions are written as ratios of numerator and denominator functions,

$$\left[G_1(s)\ G_2(s)\ G_3(s)\right]^T=\left[\frac{N_1(s)}{P(s)}\ \frac{N_2(s)}{P(s)}\ \frac{N_3(s)}{P(s)}\right]^T \tag{20}$$

they can be derived using (19) as,

$$P(s)=s^3+\left[1/(RC_f)\right]s^2+\frac{1}{L}\left[(1-D)^2/C_f+1/C_u\right]s+\left[\frac{1}{LC_uC_fR}\right] \tag{21}$$

$$N_1(s)=-\frac{1}{(LC_uC_fR)}\left[(C_fRX_3)s+(X_3+(1-D)RX_2)\right] \tag{22}$$

$$N_2(s)=\frac{s}{(LC_fR)}\left[(C_fRX_3)s+(X_3+(1-D)RX_2)\right] \tag{23}$$

$$N_3(s)=-\frac{1}{(LC_uC_f)}\left[(LC_uX_2)s^2-((1-D)C_uX_3)s+X_2\right] \tag{24}$$

Since x_3 is the output variable, the output transfer function is given by, $G_3(s)=\dfrac{N_3(s)}{P(s)}=\dfrac{-X_2}{C_f}\cdot\dfrac{(s-z_1)(s-z_2)}{(s-p_1)(s-p_2)(s-p_3)}$ (25)

where p_1, p_2 and p_3 are the system poles and z_1 and z_2 are the system zeros.

A. Exact Values of Poles in Open-Loop System

The characteristic equation of the open-loop system is given by $P(s)=0$. It can also be written as,

$$\left(LC_uC_fR\right)s^3+(LC_u)s^2+R\left[C_u(1-D)^2+C_f\right]s+1=0 \tag{26}$$

According to (26), system open-loop poles do not depend on the steady-state values of state variables. It depends only on the steady-state value of the duty-ratio and the circuit parameters. Analytical expressions for the three poles of the open-loop system can be derived by using a symbolic mathematical routine such as 'solve' of symbolic mathematics toolbox of Matlab. However, the resulting expressions are too complex for any practical analysis and therefore are not given here. Instead, approximate pole positions can be derived by considering the low frequency and high frequency behaviour of the system separately.

B. Approximate Value of Low-Frequency Pole:

Due to the complexity of analytical expressions of exact values of poles, two possible approximations are proposed in this section.

1. Approximation 1:

Since $C_u \gg C_f$ in practical converter systems, it is reasonable to neglect C_f in (26) if the duty ratio satisfies the condition, $C_u(1-D)^2 \gg C_f$, i.e.

$$D \ll 1-\sqrt{\frac{C_f}{C_u}} \tag{27}$$

The resulting characteristic equation for low frequency behaviour can be expressed as,

$$(LC_u)s^2+RC_u(1-D)^2s+1=0 \tag{28}$$

The two poles corresponding to this equation can be written as,

$$p_1^* = \frac{-R(1-D)^2}{2L}\left[1-\sqrt{1-\frac{4L}{C_u\left(R(1-D)^2\right)^2}}\right] \quad (29)$$

$$p_4^* = \frac{-R(1-D)^2}{2L}\left[1+\sqrt{1-\frac{4L}{C_u\left(R(1-D)^2\right)^2}}\right] \quad (30)$$

It can be found that the term within the square root sign is positive and the two poles are real as long as the duty ratio is below a certain limit value given by,

$$D_{c1} = 1-\sqrt{\frac{2}{R}\sqrt{\frac{L}{C_u}}} \quad (31)$$

However, considering the practical values for the circuit parameters it can be seen that D_{c1} is very close to unity. Since such high duty ratios are impractical and also violate the condition in (27), it is reasonable to assume that the two poles are real and negative in the practical range of duty ratio. Out of the two poles on the real axis of Left Half Plane (LHP) of complex s-plane, p_1^* has a small negative value and p_4^* has a large negative value, i.e. $\left|p_1^*\right| \ll \left|p_4^*\right|$. Since p_4^* is out of the focused low frequency range, it should be ignored and only p_1^* should be taken as the possible approximate value of the low frequency pole of the system.

2. Approximation 2:

If necessary, (29) can be expressed in terms of initial state values by noting in (9) and (10) that $R(1-D)^2 = X_1 / X_2$. The equation can be further simplified by approximating the term within square root sign as $\sqrt{1-x} \approx 1-\frac{x}{2}$ since x<1 when $D < D_{c1}$.

$$p_1^{**} = \frac{-X_1}{2LX_2}\left[1-\left(1-\frac{1}{2}\left\{\frac{4L}{C_u\left(X_1/X_2\right)^2}\right\}\right)\right] = \frac{-X_2}{(C_u X_1)} = -\omega_0 \quad (32)$$

This result can also be verified from the differential equation $\dot{x}_1 = (-1/C_u)\cdot x_2$ that appears in (6) and (7). This equation when converted to s-domain can be written as $sx_1 = (-x_2/C_u) \Rightarrow (s + x_2/(C_u x_1)) = 0$. Thus, the low-frequency pole at any time is given by $-x_2/(C_u x_1)$. The second possible approximate value of the pole p_1^{**} is therefore equal to $-\omega_0$ at the steady-state.

C. Approximate Values of High-Frequency Poles

Next, the characteristic equation describing the high frequency behaviour of the system can be derived by substituting $C_u \to \infty$ in (26) as,

$$s^2 + \left[1/\left(RC_f\right)\right]s + \left[(1-D)^2/\left(LC_f\right)\right] = 0 \quad (33)$$

The two poles resulting from the above equations are given by,

$$p_2^* = -1/\left(2RC_f\right) + j\sqrt{(1-D)^2/\left(LC_f\right) - 1/\left(2RC_f\right)^2} \quad (34)$$

$$p_3^* = -1/\left(2RC_f\right) - j\sqrt{(1-D)^2/\left(LC_f\right) - 1/\left(2RC_f\right)^2} \quad (35)$$

The two poles are complex conjugates with a large negative real part as long as the duty ratio is below another limit given by,

$$D_{c2} = 1-\frac{1}{2R}\sqrt{\frac{L}{C_f}} \quad (36)$$

Once again, the limiting value is very close to unity and is therefore out of the practical range.

D. Zeros of Output Transfer Function

By substituting (9) and (10) in (24), $N_3(s)$ can be expressed for running condition as,

$$N_3(s) = -\frac{X_2}{\left(C_f\right)}\left[s^2 - \left(\frac{(1-D)^2 R}{L}\right)s + \left(\frac{1}{LC_u}\right)\right] \quad (37)$$

The roots of (37) can then be derived as,

$$z_{dc1} = \frac{R(1-D)^2}{2L}\left[1-\sqrt{1-\frac{4L}{C_u\left(R(1-D)^2\right)^2}}\right] \quad (38)$$

$$z_{dc2} = \frac{R(1-D)^2}{2L}\left[1+\sqrt{1-\frac{4L}{C_u\left(R(1-D)^2\right)^2}}\right] \quad (39)$$

Note here that z_{dc1} and z_{dc2} are the zeros of the output transfer function if a dc steady-state is assumed. By comparing (38) and (39) with (29) and (30) respectively, it can be seen that $z_{dc1} = -p_1^*$ and $z_{dc2} = -p_4^*$. That means, both z_{dc1} and z_{dc2} lie on the real axis of Right Half Plane (RHP) of the complex s-plane so that $z_{dc1} \ll z_{dc2}$.

By considering the frequency shift due to the time-varying steady-state, the zeros of the output transfer function can be calculated as,

$$z_1 = z_{dc1} - \omega_0 = -p_1 - \omega_0 = \omega_0 - \omega_0 = 0 \quad (40)$$

$$z_2 = z_{dc2} - \omega_0 = \left(\frac{X_1}{LX_2} - \omega_0\right) - \omega_0 = \frac{X_1}{LX_2} - 2\omega_0 \quad (41)$$

Hence, for all practical purposes, the zero z_1 can be treated as at the origin. The remaining zero z_2 lies on the real positive axis of s-plane far away from the origin. Consequently, all the well known problems due to RHP zero of a classical boost converter, such as undershooting and limitations on controller gain, [13,14] are expected to remain the same when supplied with a bank of ultracapacitors.

E. Comparison with the Converter Supplied By a Constant Voltage Source

Conventionally, batteries with relatively constant voltage were used to supplement energy in applications where ultracapacitor banks are currently being used. Therefore, it is important to make a comparison of pole zero positions due to these two types of energy sources. The appearance of one RHP zero and the corresponding undershooting in the step response of the classical boost converter supplied by a constant voltage source are well documented [14]. The same information can be derived here by making $C_u \to \infty$ in the pole zero expressions derived for the ultracapacitor based converter.

As given by (29) and (32), both the approximate values of dominant pole p_1^* and p_1^{**} approaches zero as $C_u \to \infty$. Therefore p_1 and z_1 cancel with each other under this condition and disappears from the transfer function. The approximate values of high-frequency poles p_2^* and p_3^* do not change with C_u as the assumption $C_u \to \infty$ was made during the derivation of their values. Therefore, p_2 and p_3 can be identified as the two poles of the system supplied by a constant voltage source, such as a battery. Since the steady-state frequency $\omega_0 \to 0$ as $C_u \to \infty$, the zero z_2 reaches the maximum possible value when $C_u \to \infty$ is substituted in (41) as,

$$z_b = \frac{X_1}{LX_2} = \frac{R(1-D)^2}{L} \tag{42}$$

where z_b is the single zero of the constant voltage source supplied classical boost converter. Thus, the small-signal transfer function of the constant voltage source supplied system can be derived using (25) as,

$$G_b(s) = \frac{-X_2}{C_f} \cdot \frac{(s-z_b)}{(s-p_2)(s-p_3)} \tag{43}$$

Moreover, the zero of the ultracapacitor supplied boost converter , z_2, can be expressed in terms of z_b as,

$$z_2 = z_b - 2\omega_0 \tag{44}$$

IV. Illustrative Example

To demonstrate the control characteristics of the ultra-capacitor supplied classical boost converter, a practical system with following parameters were considered. Capacitance per cell = 100F, Number of Cells in series = 44, $\therefore C_u = 100/44 = 2.273F$, Rated Load Voltage V_r=100V, Minimum Duty Ratio D_{min}=0.1, Maximum Duty Ratio D_{max} =0.8, Converter Inductance L=4.2mH, Converter Filter Capacitance $C_f = 79\mu F$.

A. Verification of the Time-Varying Steady-State

Considering two initial values of state variables as $X_1 = 50V$, $X_3 = 100V$ and the load resistance as 10Ω, the remaining state variable, duty ratio and the steady-state frequency can be calculated using (12)-(14) as $X_2 = 20A$, $D = 0.5$, $\omega_0 = 0.176 rad/s$. Figure 2 illustrates how the three state variables vary in the steady-state if the duty ratio is kept constant at D=0.5. The simulations were performed using Matlab/Simulink. By the comparison of the simulation results with values calculated using the assumed mathematical model in (11), the high accuracy of the model given by (11) and the variables calculated using (12)-(14) can be verified.

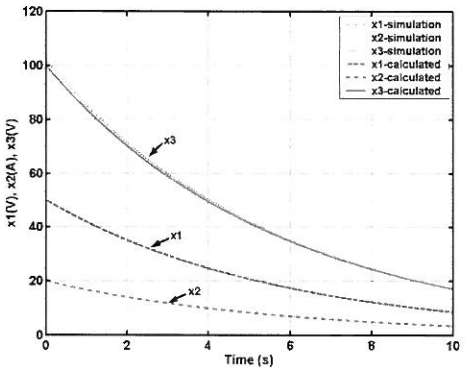

Fig.2. Simulation results and the calculated values using the assumed mathematical model for the variations of the state variables with a constant duty ratio.

B. Variations of Poles and Zero with Duty Ratio

By considering a load resistance of 22.22Ω corresponding to a rated load current of 4.5A, the critical values of duty ratios can be determined using (22) and (26) as, $D_{c1} = 0.938$ and $D_{c2} = 0.836$ respectively. Since $D_{max} < D_{c1}$, the pole p_1 will be real and negative throughout the operating range. Similarly, $D_{max} < D_{c2}$ means that the two poles p_2 and p_3 will be complex conjugates with negative real parts for the entire operating range. In order to study the effects of changing duty ratio on the system poles and zeros and also to study the sizes of errors in their approximate values, the duty ratio is changed in the operating range from 0.1 to 0.8. Figure 3(a) illustrates how the exact values of poles p_1, p_2 and p_3, calculated by solving (26), and the zero z_2 vary with the duty ratio. This figure clearly shows that the zero has the highest frequency during most of the range of duty ratio. The zero moves closer to origin as the duty ratio is increased. The pair of high frequency poles p_2 and p_3 does not appear to move closer to origin as the duty ratio is increased. Furthermore, compared to the pair of high frequency poles, the magnitude of dominant pole in the entire range of duty ratio is seen to be nearly zero.

Through the study made by changing the duty ratio, it is also possible to estimate the accuracy of approximate values of poles and zeros. The percentage errors of two approximate values of the dominant pole p_1^* and p_1^{**}, the zero z_1, the real

and imaginary parts of approximate value p_2^* are plotted against the duty ratio in Fig. 3(b). As observed from this figure, the errors of all the values except that of z_1 are below 0.1% during the full range of duty ratio. In the case of z_1 the error is up to 0.2%. As the derived equations suggested, all the errors increase with increasing duty ratio. Interestingly, the error of the second approximation of the dominant pole p_1^{**} is less than that of p_1^* and is nearly zero up to a duty ratio of about 0.7. Therefore, the dominant pole can be approximated with high accuracy by $p_1^* = -\omega_0$. Since the error in approximation of both zeros is the same, the error of z_2 is not shown in the figure. In brief, all the approximated values are highly accurate and suitable for the purpose of designing controllers. Through several case studies, it was confirmed that the pole-zero variations and the accuracy of approximation of poles are typical to most practical converter systems.

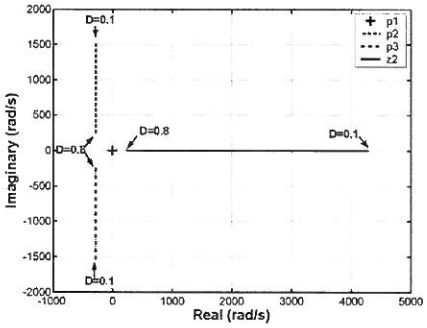

(a)

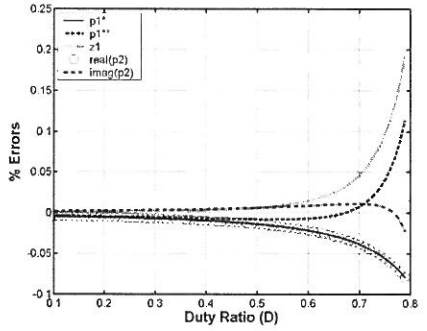

(b)

Fig. 3 Effects of Varying Duty Ratio (a) all poles and zero (b) percentage errors of approximate values.

V. Conclusions

Due to the increasing industrial applications of ultracapacitors, it is imperative to understand the characteristics of power electronic converters when supplied by banks of ultracapacitors. The variable-voltage at the terminals make the control characteristics of such systems to be significantly different from those supplied by constant voltage sources such as batteries. Based on a time-varying steady-state, system transfer functions, their poles and zeros are derived in this paper for a classical boost converter supplying a resistive load. In order to reduce the mathematical complexity, simple equations have been derived to yield highly accurate approximate values for poles and zeros. By deriving the corresponding transfer function for a constant voltage source supplied converter, it clearly demonstrates that the main difference between them is the presence of a low-frequency pole on LHP and a zero at the origin in the ultracapacitor-supplied system transfer function. Through the approximate values derived, it shows that the additional pole is due to the capacitive nature of the source. Hence the additional pole is expected to be present in general in the transfer functions derived for any power electronic converter supplied by a bank of ultracapacitors.

References

[1] B. E. Conway, *Electrochemical supercapacitors : scientific fundamentals and technological applications*, New York: Kluwer Academic / Plenum Press, 1999.

[2] A. Burke, "Ultracapacitors: why, how, and where is the technology," *Journal of Power Sources*, vol. 91, pp. 37-50, 2000.

[3] R. Kotz and M. Carlen, "Principles and applications of electrochemical capacitors," *Electrochimica Acta*, vol. 45, pp. 2483 - 2498, 2000.

[4] M. Corley, J. Locker, S. Dutton, and R. Spee, "Ultracapacitor-based ride-through system for adjustable speed drives," 30th Annual IEEE Power Electronics Specialists Conference, 1999.

[5] A. Schneuwly, M. Bärtschi, V. Hermann, G. Sartorelli, R. Gallay, and R. Kötz, "BOOSTCAP Double-Layer Capacitors for Peak Power Automotive Applications," Second International Advanced Automotive Battery Conference, 2002.

[6] J.S. Lai, S. Levy, and M. F. Rose, "High energy density double-layer capacitors for energy storage applications," *IEEE Aerospace and Electronic Systems Magazine*, vol. 7, pp. 14-19, 1992.

[7] J. L. Duran-Gomez, P. N. Enjeti, and A. von Jouanne, "An approach to achieve ride-through of an adjustable-speed drive with flyback converter modules powered by super capacitors," *IEEE Transactions on Industry Applications*, vol. 38, pp. 514-522, 2002.

[8] M. P. Kaâzmierkowski, R. Krishnan, and F. Blaabjerg, *Control in power electronics : selected problems*, Amsterdam, Boston Academic Press, 2002.

[9] R. W. Erickson and D. Maksimoviàc, *Fundamentals of power electronics*, 2nd ed. Chapman & Hall, New York, 1997.

[10] F. Belhachemi, S. Rael, and B. Davat,"A physical based model of power electric double-layer supercapacitors","Industry Applications Conference, vol. 5,2000, pp. 3069-3076.

[11] S. Buller, E. Karden, D. Kok, and R. W. De Doncker, "Modeling the dynamic behavior of supercapacitors using impedance spectroscopy,"*IEEE Trans. on Industry Applications*, vol. 38, 2002, pp. 1622-1626.

[12] R. D. Middlebrook, "Small-signal modeling of pulse-width modulated switched-mode power converters", *Proc. of the IEEE*, vol. 76, No. 4, Apr. 1988, pp. 343-354.

[13] K. J. Astrom, "Limitations on control system performance"," *European Journal of Control*", vol. 6, No. 1, 2000.

[14] K. Viswanathan, R. Oruganti, and D. Srinivasan, "A novel tri-state boost converter with fast dynamics," *IEEE Transactions on Power Electronics*, vol. 17, pp. 677-683, 2002.